Journal of Geoscience and Environment Protection, 2026, 14(1), 123-141
https://www.scirp.org/journal/gep
ISSN Online: 2327-4344
ISSN Print: 2327-4336

An Interannual Dipole Pattern of September-November Surface Maximum Air Temperature Anomalies across Tanzania and the Associated Atmospheric Conditions

Haji Suleiman Jecha[1*], Mtupili Msafiri[2,3]

[1]School of Atmospheric Sciences, Nanjing University of Information Science and Technology, Nanjing, China
[2]Key Laboratory of Virtual Geographic Environment, Ministry of Education, Nanjing Normal University, Nanjing, China
[3]School of Geographical Sciences, Nanjing Normal University, Nanjing, China
Email: *izalgebraic@gmail.com

How to cite this paper: Jecha, H. S., & Msafiri, M. (2026). An Interannual Dipole Pattern of September-November Surface Maximum Air Temperature Anomalies across Tanzania and the Associated Atmospheric Conditions. *Journal of Geoscience and Environment Protection, 14,* 123-141.
https://doi.org/10.4236/gep.2026.141008

Received: December 10, 2025
Accepted: January 19, 2026
Published: January 22, 2026

Abstract

This study presents a comprehensive analysis of the spatio-temporal patterns and governing mechanisms of September-November (SON) maximum temperature (Tmax) variability across Tanzania from 1979 to 2024. Climatologically, SON is the hottest season for Tanzania's interior, characterized by a strong thermal gradient from the persistently hot central plateau (mean Tmax > 32˚C) to the moderated coastal zones and cool highlands. Empirical Orthogonal Function analysis of SON Tmax anomalies reveals a dominant, spatially uniform pattern and a robust dipole pattern critical for interannual extremes. This dipole features out-of-phase Tmax anomalies between the central/southern interior and the northeastern/coastal regions. Correlation analysis shows the interannual component of this dipole mode (PC2) exhibits distinct extreme events but weak collective linear forcing from standard tropical climate indices (explained variance ~7.8%), with its strongest but highly non-stationary contemporaneous link to the NINO12 index. Lagged correlations suggest indices like the Dipole Mode Index may act as precursor forcings. Physically, the positive dipole phase is initiated by increased surface net longwave radiation, driven by anomalous cloudiness from modulated atmospheric dynamics. Anomalous low-level easterly/northeasterly winds transport warm, moist air from the Indian Ocean, leading to lower-tropospheric moistening, ascent above 700 hPa, and enhanced cloud cover that alters surface radiation. The increased net radiative energy is partitioned preferentially into sensible heat flux, directly warming the near-surface air. These findings underscore that regional heat extremes are shaped by a complex interplay of remote telecon-

nections and local circulation-cloud-radiation interactions, with implications for forecasting and projecting extreme heat over Tanzania's vulnerable interior.

Keywords

Maximum Temperature, Climate Variability, September-November (SON), Atmospheric Circulation, Surface Energy Fluxes, Cloud-Radiation Feedback

1. Introduction

Tanzania's climate is intrinsically linked to the socio-economic well-being of its population. Agriculture, a sector that employs a majority of the workforce, is predominantly rain-fed and highly sensitive to thermal extremes (Rowhani et al., 2011; Manatsa et al., 2020; Nkunzimana et al., 2021). The September-November (SON) season, represents a critical period in the agricultural calendar, marking the transition from the cool dry season to the onset of the shorter rains. Surface air temperature, particularly the surface maximum air temperature (Tmax), is a fundamental climate variable that directly influences evaporative demand, crop phenology and water resource availability (Lobell et al., 2011). The spatial distribution of temperature across Tanzania is well-documented as heterogeneous, governed by complex interactions between topography, proximity to the Indian Ocean, and land cover (Lyon & DeWitt, 2012). The central plateau typically experiences the highest temperatures, while the coasts and highland areas are moderated by maritime influences and altitude, respectively.

While significant researches (e.g., Nicholson, 2017; Ongoma et al., 2018; Ogwang et al., 2021; Hoell et al., 2017) have focused on precipitation variability and its associated droughts and floods over East Africa, a comprehensive understanding of the drivers of interannual temperature variability, especially during SON, remains comparatively under-explored. On an interannual timescale, East African climate is strongly modulated by large-scale modes, most notably the El Niño-Southern Oscillation (ENSO) and the Indian Ocean Dipole (IOD) (Black et al., 2003; Schreck & Semazzi, 2004). These modes exert a profound influence on regional atmospheric circulation, often leading to coherent, large-scale anomalies; for instance, El Niño events are generally associated with warmer-than-average conditions over much of East Africa (Behera et al., 2005; Anyah & Semazzi, 2007). However, this remote external forcing may obscure significant regional heterogeneity. While the physical relationship between cloud cover, surface energy fluxes, and temperature is well-established (Dai et al., 1999; Trenberth et al., 2009), a detailed observation-based analysis linking these processes to a specific mode of temperature variability over Tanzania has not been undertaken. Understanding contemporary drivers of temperature variability is a critical foundation for assessing future risks, especially given observed changes in climate extremes over the region (Omondi et al., 2014) and projected warming under global climate

change (Osima et al., 2018). Consequently, key questions remain: What are the dominant modes of interannual SON Tmax variability in Tanzania? what are the roles of atmospheric anomaly fields in driving this variability?

The novelty of this study lies in identifying a dominant regional dipole mode in SON Tmax anomalies at interannual timescales, which agrees well Tmax's climatology pattern, as well as its possible physical drivers. We move beyond merely describing the spatial pattern to reveal the full chain of mechanisms from large-scale atmospheric circulation and vertical motion, through cloud-radiative effects, to the final partitioning of surface energy fluxes. This allows us to demonstrate that the dipole pattern, characterized by opposing temperature anomalies between the interior and the coast is a physically coherent phenomenon driven by anomalous atmospheric fields in the interior. Quantifying this pathway, our work provides a mechanistic explanation for a previously underexplored aspect of Tanzania's climate variability. The specific objectives of this research are: 1) to characterize the spatio-temporal distribution and identify the dominant modes of interannual variability of SON Tmax over Tanzania, and 2) to diagnose the role of atmospheric circulation, clouds, and surface energy fluxes in driving the principal modes of variability, with a focus on elucidating the physical pathway of the identified regional dipole pattern. By unraveling these mechanisms, this work aims to contribute to a process-based understanding of regional climate variability, thereby providing a scientific basis for improved seasonal forecasting and more targeted climate risk management in Tanzania.

2. Material and Methods

2.1. Study Area and Data Sources

Tanzania, located in East Africa between 1˚S to 12˚S latitude and 29˚E to 41˚E longitude, exhibits complex topography ranging from coastal plains to the high-altitude regions of Mount Kilimanjaro and the Southern Highlands (**Figure 1**). This topographic diversity creates multiple climatic zones, from humid coastal areas to semi-arid interior regions, making it an ideal region for studying climate variability (Lyon & DeWitt, 2012). The September-November (SON) season represents a critical transition period from the dry to wet season, characterized by increasing temperatures and the onset of seasonal rains. The study utilized surface maximum air temperature (Tmax) data from the Climate Prediction Center (CPC) during 1979-2024. This dataset provides comprehensive spatial coverage with sufficient temporal resolution for analyzing interannual variability (Xie et al., 2007). For investigating physical mechanisms, we employed ERA5 reanalysis data (Hersbach et al., 2020) with the same temporal coverage, including latent heat flux, sensible heat flux, surface longwave (LW) and shortwave (SW) radiation, cloud cover, and atmospheric variables such as wind, humidity, and vertical velocity. Reanalysis data have been widely validated for climate studies in tropical regions and provide physically consistent representations of atmospheric processes (Dee et al., 2011).

2.2. Methodology

2.2.1. Analysis of Dominant Modes for SON-Mean Tmax

Empirical Orthogonal Function (EOF) analysis is employed to identify the dominant modes of interannual variability in SON Tmax across Tanzania, which has been widely used in climate studies (Björnsson & Venegas, 1997; von Storch & Zwiers, 1999). The EOF approach decomposes the spatio-temporal temperature field into orthogonal patterns that maximize the explained variance. Prior to the EOF analysis, the seasonal means are calculated from monthly Tmax data and the climatological annual cycle is removed to obtain anomalies. The covariance matrix is used for the EOF decomposition to preserve the physical units and magnitude of temperature variability. The significance of separated EOF modes is evaluated using Jones et al.'s (2020) rule of thumb, ensuring that the reported modes represent distinct signals rather than sampling errors. The principal components (PCs) associated with each EOF pattern were subsequently analyzed to understand the temporal evolution of each mode, with a particular focus on the interannual variability in this study.

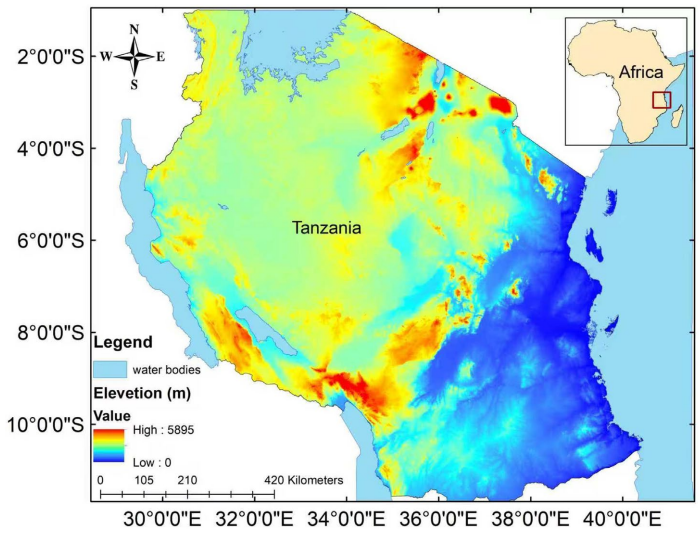

Figure 1. Shaded relief map of Tanzania, indicating variations in land surface elevation. The highest point is Mount Kilimanjaro at 5895 meters above sea level (Source: Author).

2.2.2. Composite Analysis of Atmospheric Circulation

Composite analysis is conducted to elucidate the atmospheric conditions associated with different phases of the identified Tmax variability modes. Years with PCs out of the range of ±0.5 standard deviation (s.d.) are selected to create composites for high (higher than +0.5 s.d.) and low (lower than −0.5 s.d.) PC years, following established methodologies in climate dynamics research (Goddard & Graham, 1999). This threshold provides a balance between maintaining adequate sample size and ensuring clear separation between opposing phases. Statistical significance of composite anomalies or differences is assessed using Student's t-test, with adjustments for effective sample size due to temporal autocorrelation (Wilks, 2011).

2.3. Surface Energy Flux Analysis

This analysis of surface energy budget is carried out independently by assessing individual flux components to isolate their specific roles in driving temperature variability (Trenberth et al., 2009). Please note that all the fluxes and radiation in ERA5 are positive downward, which means a positive contribution signifies a process adding heat to the surface (warming) and a negative contribution signifies heat removal (cooling). Thus, net shortwave radiation remains a primary positive (warming) driver, while the typically upward net longwave radiation is explicitly isolated as a persistent negative (cooling) contributor. The turbulent fluxes are similarly interpreted upward sensible and latent heat fluxes (convection and evaporation) represent negative (cooling) contributions, with a reversal to downward fluxes indicating a positive (warming) effect. This sign-aware decomposition allows the attribution of temperature variability to distinct physical mechanisms radiative, turbulent, latent and conductive providing a clearer process-based diagnosis than analyzing the net energy balance alone.

3. Results

3.1. Spatio-Temporal Distribution of Maximum Temperature across Tanzania

The spatial analysis of monthly mean Tmax across Tanzania from 1979 to 2024 reveals a distinct and dynamic climatological pattern (**Figure 2**). The central plateau region, encompassing much of the Dodoma and Singida, consistently exhibits the highest temperatures throughout the year, with mean Tmax values frequently exceeding 32˚C. The hottest conditions are observed in the months leading up to the primary rainy season, particularly from October to December, where the central interior experience mean Tmax values reaching 34˚C or higher (**Figures 2(j)-(l)**). In contrast, the eastern and southern coastal zones, including Dar es Salaam and Mtwara, along with the offshore islands of Zanzibar and Mafia, display a more moderated and stable thermal regime with mean Tmax values ranging between 28˚C and 31˚C across all months. The mountainous regions in the northeast (Kilimanjaro) and southwest (Mbeya) persistently show the coolest conditions, with mean Tmax consistently below 26˚C. During the peak of the dry season, from June to September, the band of highest temperatures expands, covering much of the central and southern inland regions (**Figures 2(f)-(i)**). Conversely, the central rainy season from March to May brings a noticeable cooling effect to the interior (**Figures 2(c)-(e)**). However, this cooling is less pronounced along the coast, which maintains its relatively stable temperatures year-round.

This annual cycle ends in the SON season, which represents the transitional period from the cool and dry season to the hot and wet season (**Figure 3**). The spatial average for this season consolidates the patterns showing a strong thermal gradient from the hot central plateau to the cooler coastal and highland fringes. The central region remains the thermal center of the country during SON, with spatially averaged Tmax values firmly in the range of 32˚C - 34˚C. This confirms

that SON is the hottest quarter of the year for the majority of Tanzania's interior, setting the stage for the onset of seasonal rains.

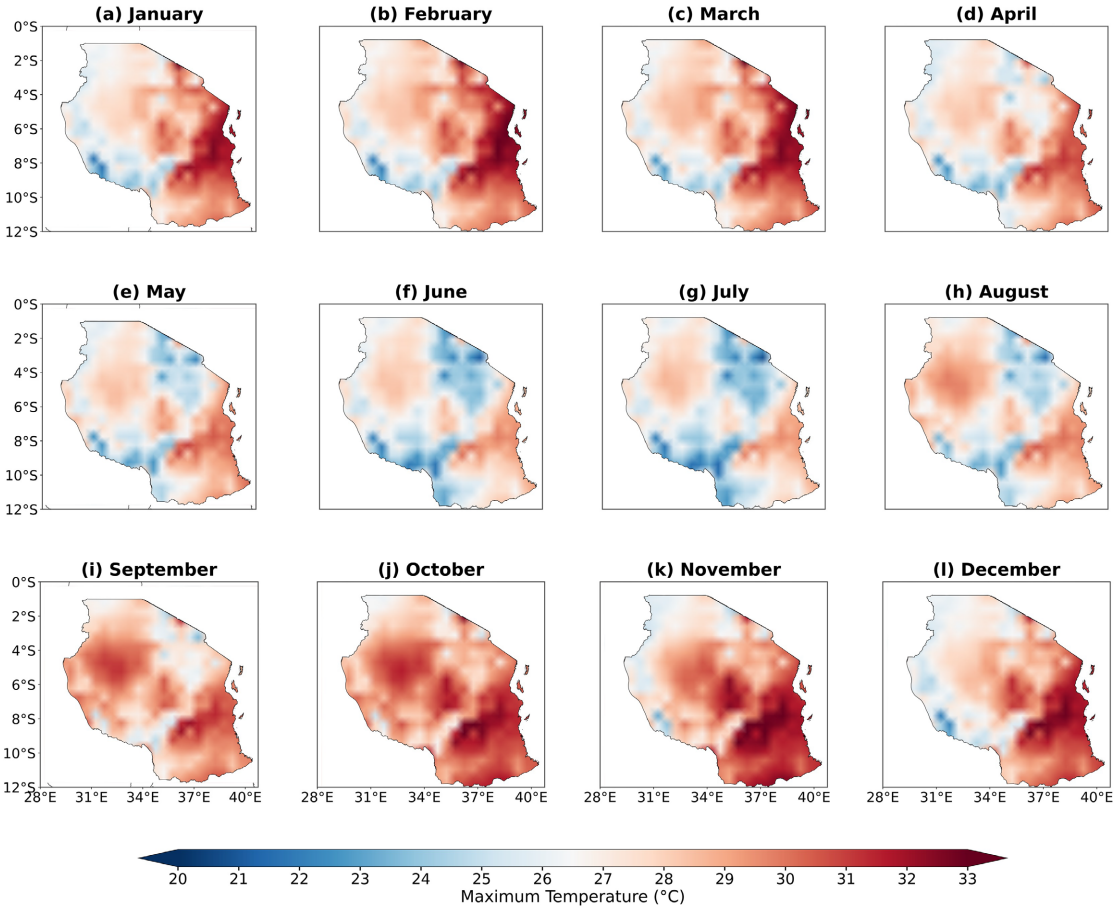

Figure 2. Spatial distribution of monthly mean Tmax (in ˚C) across Tanzania during 1979 to 2024 based on CPC from (a) January to (l) December.

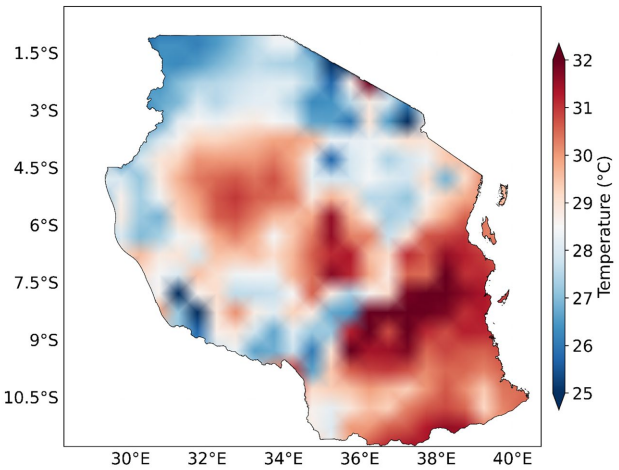

Figure 3. Seasonal distribution of Tmax (in ˚C) over Tanzania averaged from September to November (SON) during 1979 to 2024.

3.2. Dominant Modes of SON Tmax Variability across Tanzania

The first leading EOF mode (EOF1) accounts for 41.1% of the total variance, which demonstrates that the most significant driver of interannual temperature anomalies is a uniform and nationwide warming or cooling (Figure 4(a)). However, the second EOF mode (EOF2) accounts for 21.4% of the total variance. Interestingly, EOF2 shows a dipole pattern of Tmax anomalies, with a strong contrast between the central interior and the northeast/coast (Figure 4(b)). Clearly, this EOF2 mode spatially agree with the climatology pattern of SON Tmax, especially for the Tmax center over the central interior region (comparing Figure 4(b) to Figure 3). This spatial agreement would allow us to explore the interannual variability of Tmax over the central plateau based on the EOF2 mode, rather than EOF1 with anomalous Tmax center over the mountain region in the southwest. Thus, our focus is on the EOF2 pattern (i.e., the dipole pattern) and its associated atmospheric anomaly conditions in the following.

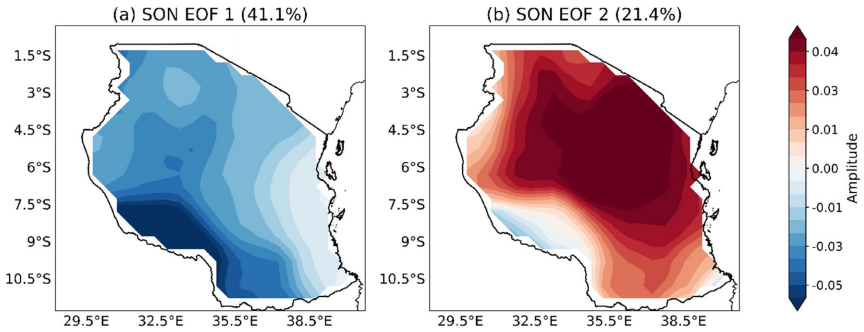

Figure 4. The leading Empirical Orthogonal Function (EOF) modes for the SON-mean Tmax from 1979 to 2024: (a) the first EOF mode (EOF1) and (b) the second EOF mode (EOF2).

Figure 5 shows the principal component time series of the dipole mode (i.e., PC2). Clearly, there exist certain inter-decadal variations (Figure 5(a), red line) of this mode, suggesting possible low-frequency oscillations that may modulate the frequency or intensity of this dipole pattern over multi-year periods. More critically, the inter-annual component (Figure 5(b), green line) allows for the identification of specific years where this mode is strongly active. According to interannual time series of PC2, ten high years are identified as 1980, 1981, 1987, 1993, 2003, 2005, 2016, 2017, 2018 and 2021, and nine low years are identified as 1982, 1984, 1989, 1994, 1997, 1999, 2006, 2019 and 2020.

The physical reality and impacts of this dipole can be confirmed by the composite analysis (Figure 6). During years with a strong positive PC2, the central and southern interior experiences significant positive Tmax anomalies mostly exceeding +1.0˚C, while the southwest and coastal regions show weak warming or even slight cooling (Figure 6(a)). Conversely, during strong negative PC2 years, the pattern is opposite with the interior cooling and the coastal/southwestern regions warming (Figure 6(b)). The difference map highlights this dipole pattern and confirms that the contrasting anomalies between the two regions are statistically

significant (Figure 6(c)). As shown later, this seesaw effect is likely driven by regional anomaly patterns of atmospheric circulation and clouds.

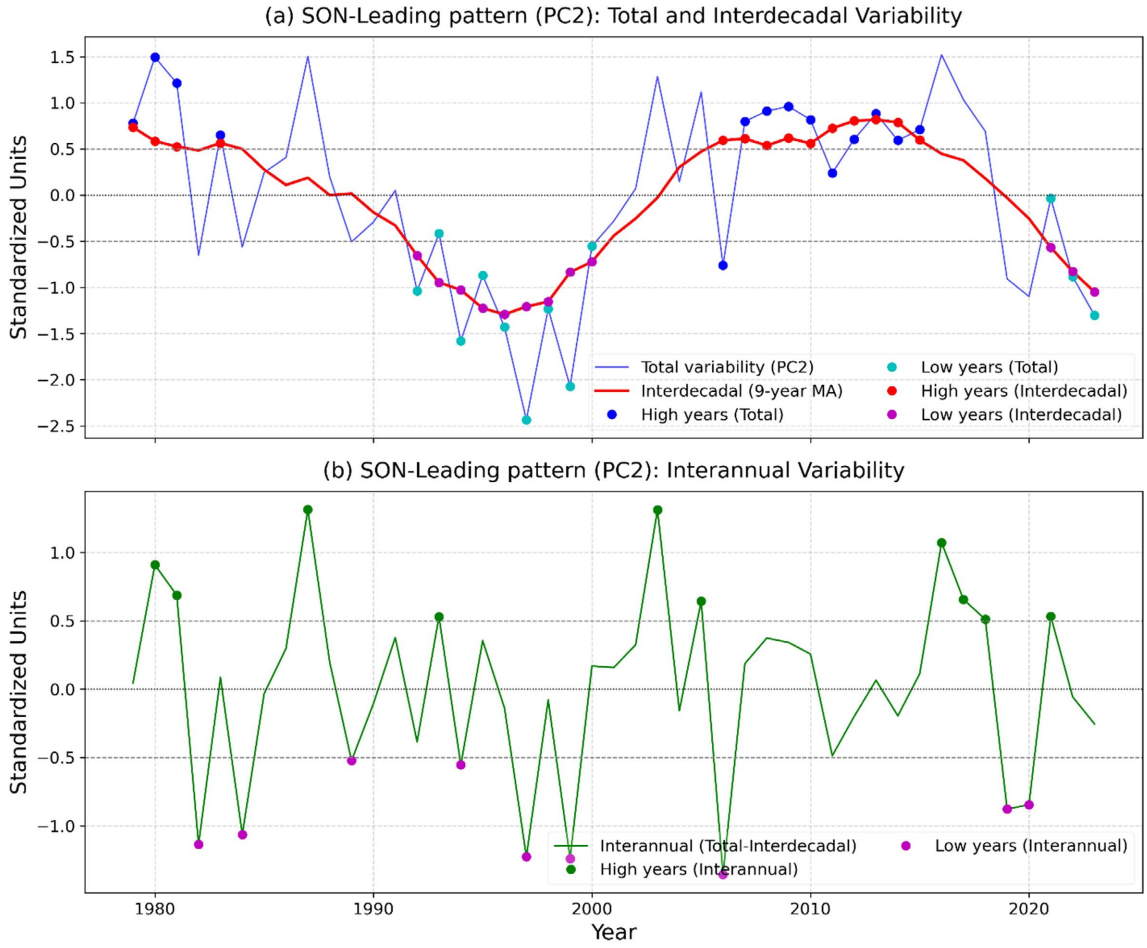

Figure 5. Principal component of the EOF2 (PC2): (a) total variability (blue line) and inter-decadal variability (9-year moving average, red line) and (b) inter-annual variability (calculated as total minus inter-decadal components, green line; referred to as PC2).

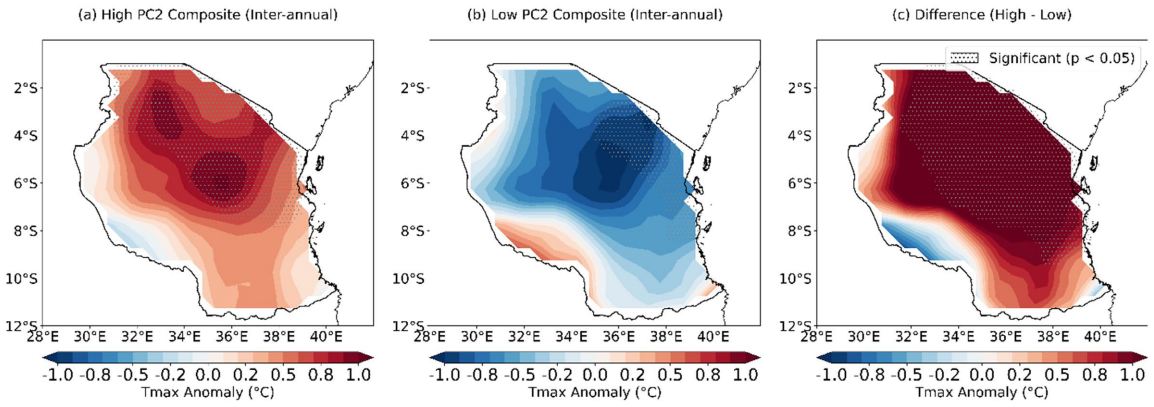

Figure 6. Composites of the interannual anomalies of SON-mean Tmax based on extreme years of PC2 for (a) high years, (b) low years, and (c) their difference (i.e., high years minus low years; (a) minus (b)). The stippling indicates the difference is statistically significant with $p < 0.05$ based on Student's t test.

3.3. Physical Mechanisms Driving the Variability of SON Tmax Temperature across Tanzania

3.3.1. The Correlation Analysis between the Interannual Component of PC2 and Standard Climate Indices

The results of the analysis of the SON PC2 time series reveals a climate mode with distinct extreme events but weak linear forcing from common tropical indices (Figure 7). The standardized time series in panel (a) identifies specific extreme years where PC2 exceeded ±1.0 standard deviations, with notable positive peaks including 1998, 2010, and 2020 (Figure 7(a)); these eight highs and seven low extremes form the basis for the composite analysis (Figure 7(h)). Despite of the clarity of these events, a multivariate linear regression using six indices (DMI, NINO12, NINO34, NINO4, IOD, SOI) explains only 7.8% of the total variance in PC2, indicating a very weak collective linear influence (Figure 7(d)). The strongest individual contemporaneous teleconnection is with the NINO12 index, as shown by the correlation analysis and the scatter plot (Figure 7(b), Figure 7(c)). This is quantified where NINO12 contributes the largest portion of the individually explained variance (Figure 7(i)). However, the 15-year running correlation demonstrates that this relationship with NINO12 is highly non-stationary, shifting markedly over recent decades and suggesting that the identified extreme years are not consistently tied to a single ENSO phase (Figure 7(g)). Furthermore, the lagged correlation diagnostics in panel (f) reveal that indices such as the DMI/IOD exhibit significant correlations when leading PC2 by several months, indicating they may act as precursor forcing mechanisms for extreme PC2 events (Figure 7(f)). The SON PC2 mode is characterized by strong episodic extremes but appears to be driven by a complex, evolving interplay of tropical signals, where direct contemporaneous influences are modest and often supplemented or preconditioned by lagged interactions from basins like the Indian Ocean.

3.3.2. Surface Energy Fluxes and Cloud Characteristics

Figure 8, Figure 9 show the composites of interannual anomalies of surface energy fluxes and clouds, which provide the crucial physical mechanisms that explain the distinct regional dipole pattern (EOF2) of SON Tmax variability identified above.

The key initiator of the surface heating pattern over the central interior is a significant increase in surface net LW radiation (LW_{net}) during the positive PC2 phase (Figures 8(d)-(f)). This large positive LW_{net} anomaly (exceeding +20 $W \cdot m^{-2}$) indicates substantially enhanced downwelling LW radiation at the surface. This is primarily due to increased downwelling longwave radiation (Figure not shown), likely from a warmer and more humid atmospheric boundary layer under increased cloud cover. On the other hand, surface net SW radiation (SW_{net}) increases (decreases) under high (low) PC2 years (Figures 8(a)-(c)), indicating that the Tmax change is also partially induced by the SW_{net}. Clearly, the anomaly magnitude of SW_{net} is much smaller than that of LW_{net}, suggesting a bigger role of LW_{net} in driving SON Tmax changes.

The combined increase in LW_{net} and SW_{net} provides abundant net radiative energy at the surface. This energy is partitioned primarily into sensible heat flux, which shows a large and statistically significant increase (over +10 $W \cdot m^{-2}$; Figures 8(g)-(i)). The warmed surface heats the near-surface air, and this warmer air then further warms the surface through enhanced downward sensible heat flux, creating positive feedback that amplifies maximum temperatures. Simultaneously, the latent heat flux in the interior shows a slight decrease or minimal change (Figures 8(j)-(l)), indicating that the available energy is channeled preferentially into sensible heating rather than evaporation.

Figure 7. Analysis of the second principal component (PC2) time series for September-October-November (SON) from 1979 to 2023 quantitatively correlated with climate indices. Panels shows (a) Standardized PC2 time series, highlighting extreme years (b) Correlations between PC2 and key climate indices (c) Scatter plot of the strongest correlation (d) multivariate regression coefficients (total explained variance $R^2 = 0.078$ $R^2 = 0.078$) (e) Time series of key climate Indices (f) Multifaceted diagnostics including lagged correlations (positive lag = index leads PC2), (g) 15-years running correlation between PC2 and NINO12 (h) Composite analysis for high/low PC2 years and (i) Individual explained variances.

Figure 9 shows the spatial distribution of composite of cloud cover. During high PC2 years with central warming, the central interior experiences a substantial increase of cloud cover (Figure 9(a), Figure 9(d), Figure 9(g)), which directly

explains the concurrent significant increase in LW_{net} (over +20 $W \cdot m^{-2}$; Figure 8(d)). The spatial pattern of enhanced longwave cloud forcing aligns perfectly with the positive lobe of the Tmax dipole. This further confirms that the initial and dominant radiative control mainly comes from the larger LW_{net} anomaly due to cloud changes, rather than SW_{net}.

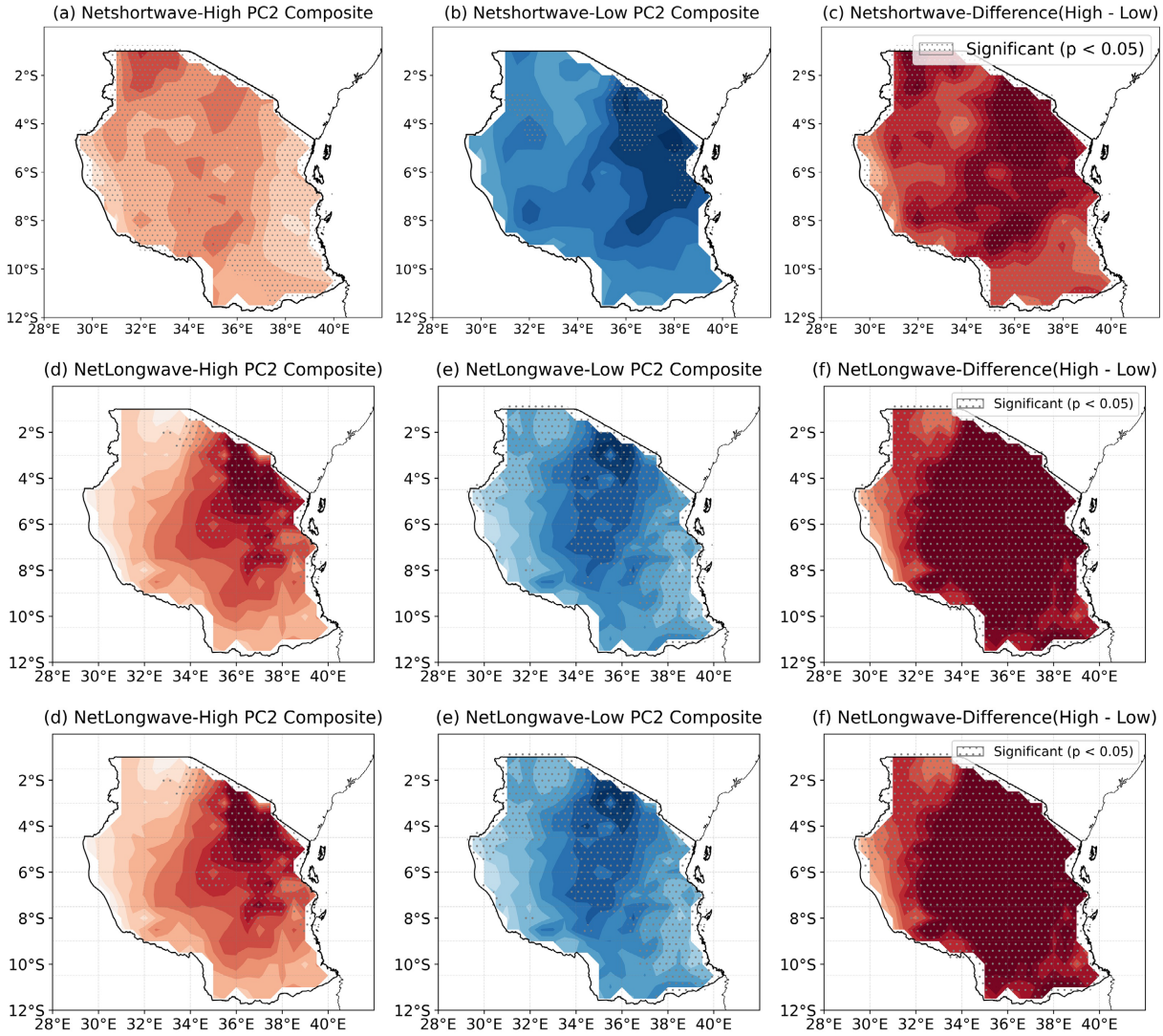

Figure 8. Composite analysis of the interannual anomalies of SON-mean (a-c) surface shortwave radiation (SWnet), (d-f) surface net longwave radiation (LWnet), (g-i) surface sensible heat flux (SSHF), (j-l) surface latent heat flux (SLHF) based on extreme years of PC2 for (a, d, g, j) high years, (b, e, h, k) low years, and (c, f, I, l) their differences (i.e., high years minus low years). All the surface fluxes and radiation are in W/m2 with positive values downward. The stippling indicates the differences are statistically significant with $p < 0.05$ based Student's t test.

Please note that the initial radiative warming in the interior can be further amplified by the land-atmosphere feedbacks. Accelerated soil drying shifts the surface energy balance from latent to sensible heat flux, a globally recognized accelerator of heat extremes (Seneviratne et al., 2010). This feedback is particularly effective in transitional climate zones like the Tanzanian interior, as demonstrated

in studies on heatwave amplification (Miralles et al., 2019) and the global sensitivity of afternoon temperatures to surface moisture (McColl et al., 2022b). Furthermore, the resulting warm, dry boundary layer enhances downwelling longwave radiation, creating a localized "greenhouse" effect that reinforces nighttime warming and event persistence, a mechanism detailed in heatwave analyses (Rasmijn et al., 2018; Perkins-Kirkpatrick & Gibson, 2017).

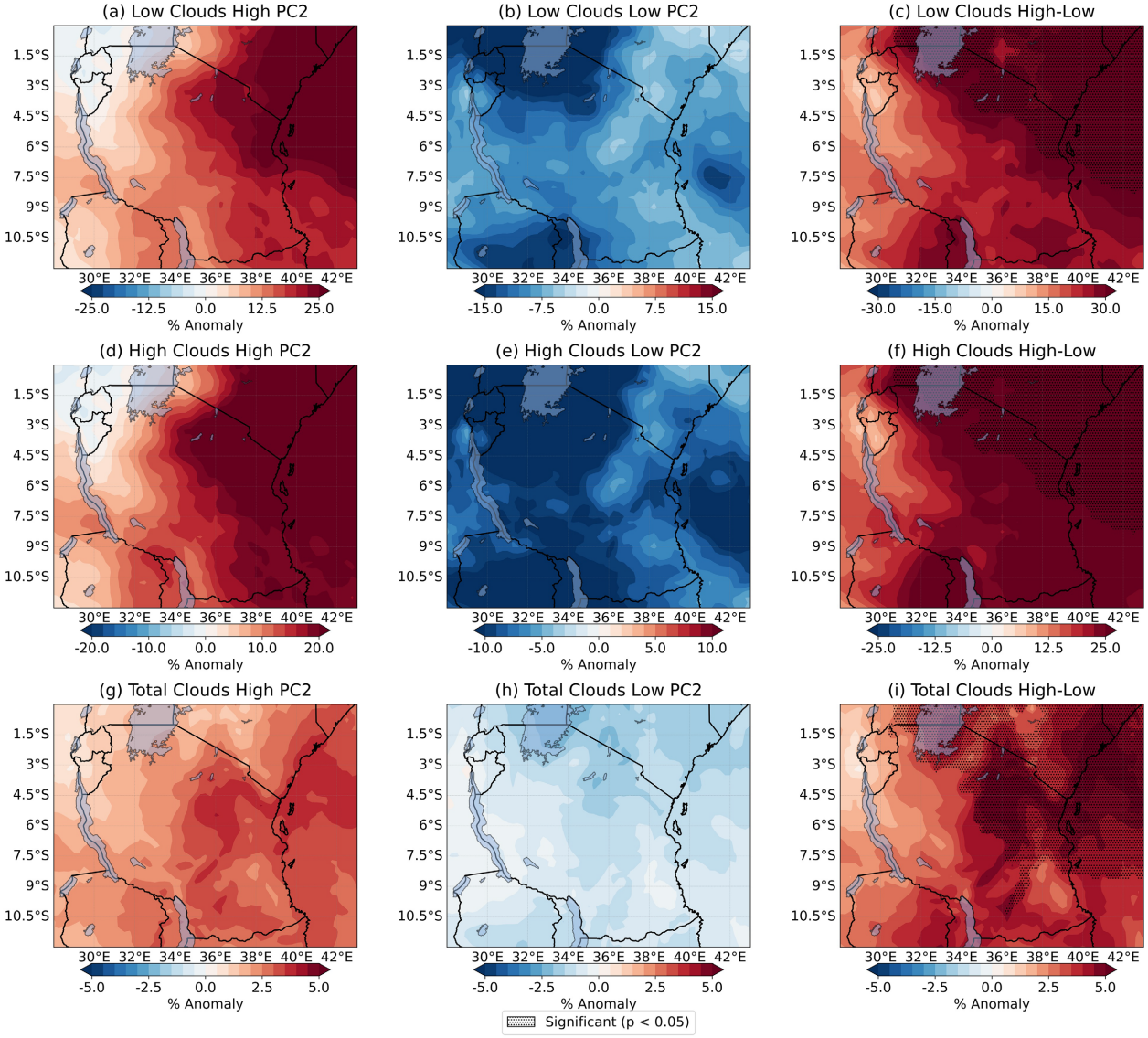

Figure 9. Composite analysis of the interannual anomalies of SON-mean (a-c) low cloud cover (in % of sky), (d-f) high cloud cover (in % of sky), (g-i) total cloud cover (in % of sky) based on extreme years of PC2 for (a, d, g) high years, (b, e, h) low years, and (c, f, i) their differences (i.e., high years minus low years). The stippling indicates the differences are statistically significant with $p <$ 0.05 based Student's t test.

3.3.3. Atmospheric Circulation, Vertical Velocity and Moisture Flux Divergence

The analysis of atmospheric circulation and moisture dynamics provides the fundamental dynamics for the cloud cover and surface energy flux patterns that drive

the SON Tmax dipole pattern (Figure 10, Figure 11). During the positive PC2 years, remarkable anomalous easterly and northeasterly winds occur over most areas of Tanzania, which advect a warm and moist oceanic air mass from the northeast into the central and southern interior regions (Figure 10(a), Figure 10(c)). Accordingly, the lower troposphere becomes moister with increased relative humidity (RH). However, at approximately 850 hPa, the central interior experiences a significant increase in moisture flux divergence during high PC2 years, where the wind field actively transports moisture away from the near-surface layer, thus desiccating the very low-level atmosphere. This low-level divergence is vertically decoupled from the dynamical forcing above it (Figure 11(a)), anomalous ascent dominates the layer from 850 hPa to 700 hPa. This ascent lifts the advected moist air, facilitating cloud formation at these higher altitudes despite the near-surface divergence. In contrast, the coastal zone shows a tendency towards moisture flux convergence at 850 hPa, consistent with the direct advection of maritime moisture and more clouds there (Figure 9(a)). As a result, there is a large increase in total cloud cover in the central interior and coastal regions, while clouds increase less in the western inland (Figure 9(g)).

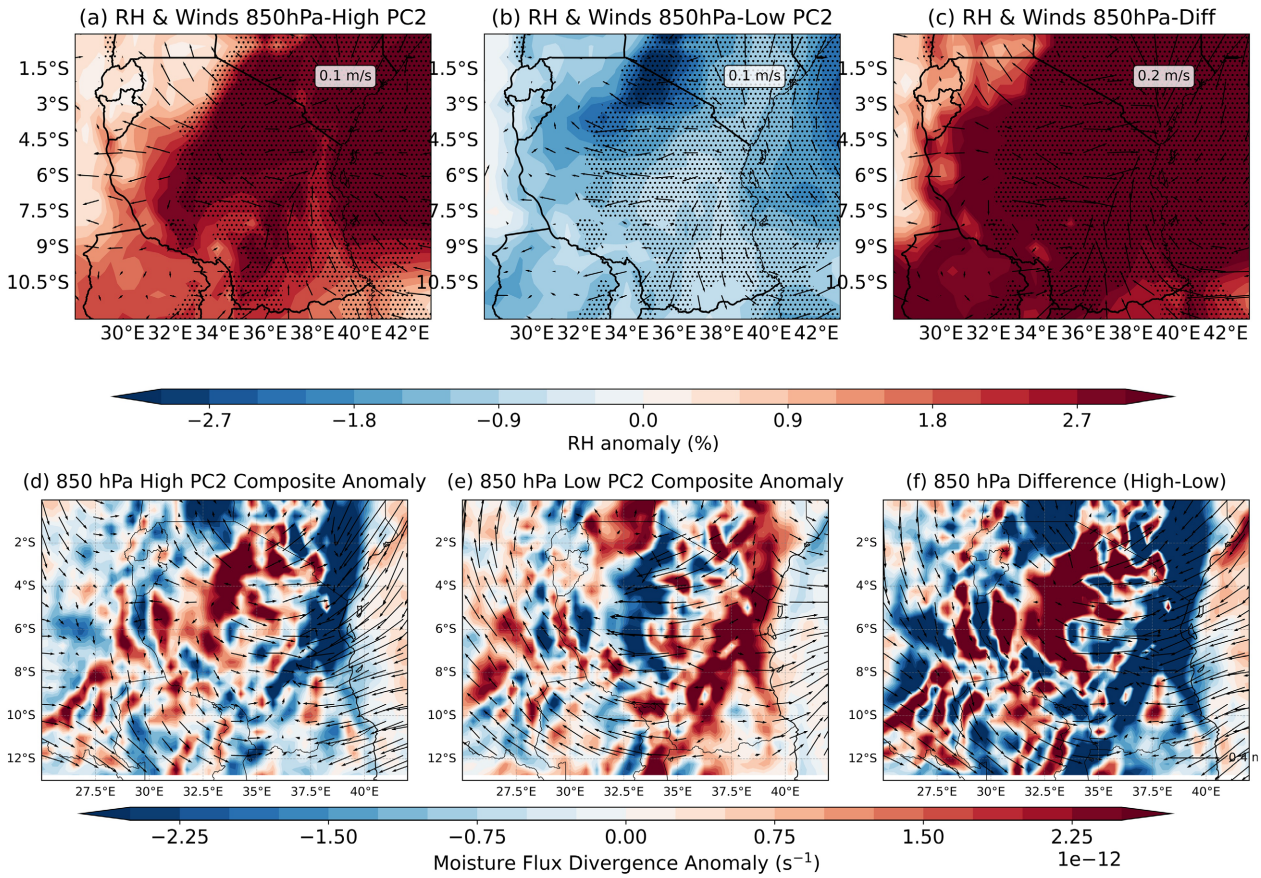

Figure 10. Composites analysis of the interannual anomalies of SON-mean (a-c) relative humidity (RH, shading, in %) and (d-f) moisture flux divergence (shading, in 1/s) at 850hPa based on extreme years of PC2 for (a & d) high years, (b & e) low PC2-IV years, and (c & f) their differences (i.e., high years minus low years), overlaid with 850-hPa wind anomalies (vectors, in m/s). The stippling indicates the differences are statistically significant with $p < 0.05$ based Student's t test.

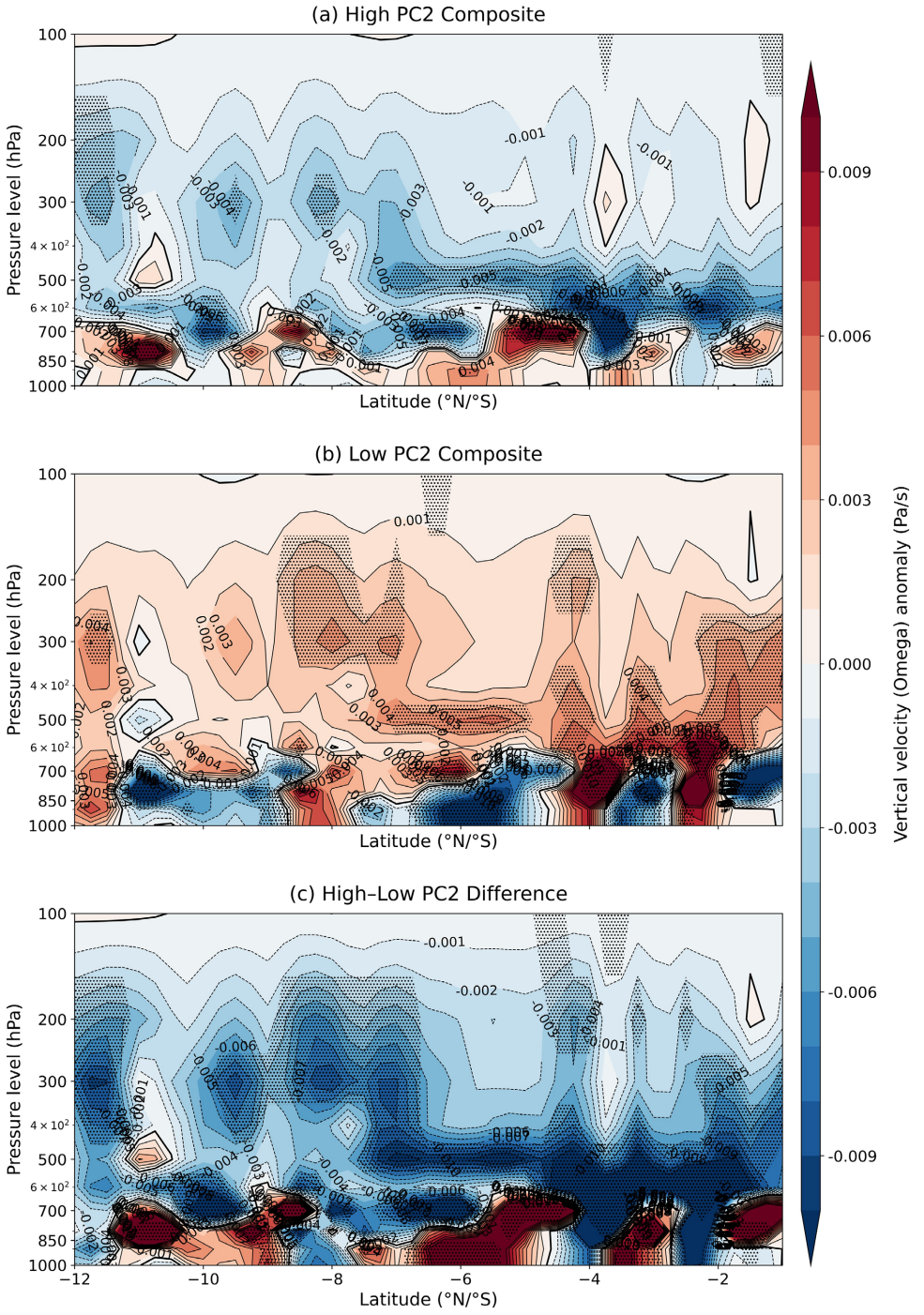

Figure 11. Analysis of the Pressure-latitude cross-sections for the composites interannual anomalies of vertical velocity (ω, in Pa/s) averaged over the 25˚ to 42˚E based on extreme years of PC2 for (a) high years, (b) low years, and (c) their difference (i.e., high years minus low years). The stippling indicates the differences are statistically significant with $p < 0.05$ based Student's t test.

3.3.4. The Potential Drivers of the Uniform Warming/Cooling Pattern of EOF1

The uniform warming/cooling pattern of EOF1, which explains the dominant share (41.1%) of SON Tmax variance is not analyzed in detail here but is a char-

acteristic of large-scale coherent mode typically associated with global background warming and pervasive sea surface temperature forcings (Seneviratne et al., 2010). This pattern is most consistent with forcings that operate synchronously across the region, primarily the long-term trend of global climate change and basin-wide sea surface temperature (SST) anomalies, such as uniform Indian Ocean basin warming or the canonical, broad-scale teleconnection from Pacific ENSO events, which can modulate atmospheric stability and cloud cover across East Africa. While EOF1 captures the most overall variance, the we focus mechanistic analysis on EOF2 (21.4% of variance) because of its dipole structure aligns with the core climatological heat center over the central plateau. This allows for an investigation of the regionally specific dynamics moisture advection, vertical motion and the cloud-radiative feedbacks that interact with powerful land-atmosphere coupling which are critical for understanding and predicting impactful temperature extremes in Tanzania's interior, a region highly sensitive to soil moisture temperature feedbacks (Miralles et al., 2019; McColl et al., 2022a; Rasmijn et al., 2018).

4. Conclusion and Discussion

This study provides a comprehensive analysis of September-November (SON) maximum temperature (Tmax) variability over Tanzania from 1979 to 2024. The key findings are as follows.

The first leading mode of interannual variability (explaining 41.1% of the total variance) exhibits a uniform and nationwide Tmax warming or cooling, while the second mode shows a dipole pattern with contrasting Tmax anomalies between the central interior and the northeast/coastal regions. Although this dipole pattern only explains 21.4% of the total interannual variance, its spatial structure aligns strongly with the climatological mean SON Tmax distribution, particularly the perennial hot center over the central plateau, which can be treated as an optimal focus for understanding interannual variability in this critical region.

The causal chain for central interior warming during the positive dipole phase involves a clear sequence: The initial driver is a radiative forcing from increased surface downwelling longwave radiation (LWdwn) due to anomalous cloud cover. This cloud increase is dynamically governed by enhanced low-level moisture advection and convergence, along with mid-level ascent, which facilitate cloud formation over the interior. Subsequently, this initial radiative warming is amplified by land-atmosphere feedbacks. The increased net radiative energy is partitioned predominantly into sensible heat flux, directly heating the near-surface air. This heating likely reinforces soil moisture depletion, further suppressing latent heat flux and creating a positive feedback loop that amplifies the initial temperature anomaly.

Analysis of the associated principal component (PC2) reveals that this dipole mode is characterized by strong episodic extremes but weak linear forcing from common tropical climate indices (**Figure 7**). A multivariate regression using six

standard indices (DMI, NINO12, NINO34, NINO4, IOD, SOI) explains only 7.8% of PC2's variance. The strongest contemporaneous teleconnection is with the NINO12 index, but this relationship is highly non-stationary, as shown by 15-year running correlations. Significant lagged correlations, particularly with the IOD/DMI, suggest that Indian Ocean conditions may act as precursor forcings for some extreme dipole events. This indicates that the large-scale circulation anomalies driving the cloud dynamics are themselves the product of a complex, evolving interplay of remote influences, rather than a simple, stationary response to a single mode like ENSO.

These findings collectively underscore the necessity of incorporating regional-scale processes specifically cloud dynamics and land-atmosphere interactions—into seasonal forecasts and climate projections for Tanzania. The identified mechanism suggests that under anthropogenic warming, potential changes in low-cloud cover may initiate radiative forcing that could then be disproportionately amplified by soil moisture feedbacks, exacerbating heat extremes in the vulnerable continental interior relative to the buffered coastline. The cloud-mediated longwave radiation initiates the surface warming aligns with mechanisms identified in other parts of Africa, where the cloud-radiative effect dominates daytime temperature variability (Kamoru et al., 2022) and this shift from latent to sensible heat flux can further desiccate soils, potentially triggering positive feedbacks known to influence afternoon boundary layer development and convective likelihood (Taylor et al., 2012). The critical role of cloud-radiative forcing highlighted here underscores the importance of accurately representing low-cloud feedbacks in models, which remains a key uncertainty for climate sensitivity projections (Myers et al., 2021). The amplified sensible heating and soil drying we identify can create conditions for persistent heat extremes, with potential legacy effects on ecosystems similar to those documented in other regions (Bastos et al., 2020).

Furthermore, the coastal zone experiences a starkly different energy budget trajectory that actively suppresses warming. The ample moisture supply from the Indian Ocean and sustained cloud cover ensure that the surface energy balance remains dominated by latent heat flux, providing a powerful buffering effect. This moderating maritime influence is mechanistically the opposite of the interior's feedback loop and is well-documented in regional modeling studies (Anyah & Semazzi, 2007; Kijazi & Reason, 2009). Consequently, the dipole emerges from this fundamental dichotomy: synergistic, positive feedbacks amplify extreme heat inland, while maritime stability and cloud albedo thermally insulate the coast. This internally coherent mechanism chain from complex remote forcing to regional circulation, cloud radiative effects, and local land-atmosphere feedbacks underscores that regional temperature extremes are not solely forced by large-scale climate modes but are powerfully shaped by local interactions. Understanding these regional drivers is urgent, as future climates are projected to intensify and expand heat stress exposure across Africa (Dajuma et al., 2024).

5. Significance Statement

This study identifies a dominant regional dipole pattern in Tanzania's hottest season (September-November), in which the central interior and coastal areas experience opposite temperature extremes. It establishes the physical mechanism by which atmospheric circulation anomalies regulate cloud cover and surface energy fluxes to drive these extremes. This process understanding is critical for enhancing climate models and seasonal forecasts of heatwaves. The findings directly support the development of targeted early warning systems and climate-resilient strategies for agriculture and public health, particularly in Tanzania's vulnerable interior.

Data Availability Statement

The monthly mean maximum temperature data used in this study are available from the NOAA Climate Prediction Center (CPC) at https://psl.noaa.gov/data/gridded/index.html, while the remaining variables comprising surface energy fluxes, radiation components, cloud cover, moisture flux divergence and 850-hPa dynamical fields are available from the ECMWF climate reanalysis at https://www.ecmwf.int/en/forecasts/datasets.

Conflicts of Interest

The authors declare no conflicts of interest regarding the publication of this paper.

References

Anyah, R. O., & Semazzi, F. H. M. (2007). Variability of East African Rainfall Based on Multiyear Regcm3 Simulations. *International Journal of Climatology, 27,* 357-371. https://doi.org/10.1002/joc.1401

Bastos, A., Ciais, P., Friedlingstein, P., Sitch, S., Pongratz, J., Fan, L. et al. (2020). Direct and Seasonal Legacy Effects of the 2018 Heat Wave and Drought on European Ecosystem Productivity. *Science Advances, 6,* eaba2724. https://doi.org/10.1126/sciadv.aba2724

Behera, S. K., Luo, J., Masson, S., Delecluse, P., Gualdi, S., Navarra, A. et al. (2005). Paramount Impact of the Indian Ocean Dipole on the East African Short Rains: A CGCM Study. *Journal of Climate, 18,* 4514-4530. https://doi.org/10.1175/jcli3541.1

Björnsson, H., & Venegas, S. A. (1997). A manual for EOF and SVD Analyses of Climatic Data. McGill University, *CCGCR Report, 97,* 112-134.

Black, E., Slingo, J., & Sperber, K. R. (2003). An Observational Study of the Relationship between Excessively Strong Short Rains in Coastal East Africa and Indian Ocean SST. *Monthly Weather Review, 131,* 74-94. https://doi.org/10.1175/1520-0493(2003)131<0074:aosotr>2.0.co;2

Dai, A., Trenberth, K. E., & Karl, T. R. (1999). Effects of Clouds, Soil Moisture, Precipitation, and Water Vapor on Diurnal Temperature Range. *Journal of Climate, 12,* 2451-2473. https://doi.org/10.1175/1520-0442(1999)012<2451:eocsmp>2.0.co;2

Dajuma, A., Sylla, M. B., Tall, M., Almazroui, M., Afiesimama, E., Dosio, A. et al. (2024). Projected Intensification and Expansion of Heat Stress and Related Population Exposure over Africa under Future Climates. *Earth's Future, 12,* e2024EF004646. https://doi.org/10.1029/2024ef004646

Dee, D. P., Uppala, S. M., Simmons, A. J., Berrisford, P., Poli, P., Kobayashi, S. et al. (2011).

The Era-Interim Reanalysis: Configuration and Performance of the Data Assimilation System. *Quarterly Journal of the Royal Meteorological Society, 137,* 553-597. https://doi.org/10.1002/qj.828

Goddard, L., & Graham, N. E. (1999). Importance of the Indian Ocean for Simulating Rainfall Anomalies over Eastern and Southern Africa. *Journal of Geophysical Research: Atmospheres, 104,* 19099-19116. https://doi.org/10.1029/1999jd900326

Hersbach, H., Bell, B., Berrisford, P., Hirahara, S., Horányi, A., Muñoz-Sabater, J. et al. (2020). The ERA5 Global Reanalysis. *Quarterly Journal of the Royal Meteorological Society, 146,* 1999-2049. https://doi.org/10.1002/qj.3803

Hoell, A., Funk, C., & Barlow, M. (2017). The Forcing of Monthly Precipitation Variability over Southern Africa during the 2015-2016 El Niño. *Journal of Climate, 30,* 9517-9539.

Jones, J. J., Bell, M. M., & Klotzbach, P. J. (2020). Tropical and Subtropical North Atlantic Vertical Wind Shear and Seasonal Tropical Cyclone Activity. *Journal of Climate, 33,* 5413-5426. https://doi.org/10.1175/jcli-d-19-0474.1

Kamoru, A. M., Lawal, K. A., & Abiodun, B. J. (2022). Dominant Role of Cloud-Radiative Effect in Governing Daytime Temperature Variability over West Africa. *Journal of Geophysical Research: Atmospheres, 127,* e2021JD035718.

Kijazi, A., & Reason, C. (2009). Analysis of the 1998 to 2005 Drought over the Northeastern Highlands of Tanzania. *Climate Research, 38,* 209-223. https://doi.org/10.3354/cr00784

Lobell, D. B., Schlenker, W., & Costa-Roberts, J. (2011). Climate Trends and Global Crop Production since 1980. *Science, 333,* 616-620. https://doi.org/10.1126/science.1204531

Lyon, B., & DeWitt, D. G. (2012). A Recent and Abrupt Decline in the East African Long Rains. *Geophysical Research Letters, 39,* L02702. https://doi.org/10.1029/2011gl050337

Manatsa, D., Mushore, T. D., & Lenouo, A. (2020). Improved Predictability of Droughts over Southern Africa Using the Standardized Precipitation Evapotranspiration index and ENSO. *Theoretical and Applied Climatology, 139,* 307-327.

McColl, K. A. et al. (2022a). Global Distribution of the Sensitivity of Land-Atmosphere Coupling to Soil Moisture. *Nature Climate Change, 12,* 775-782.

McColl, K. A. et al. (2022b). Global Spatial and Temporal Patterns of Afternoon Precipitation and Its Sensitivity to Surface Moisture. *Nature Geoscience, 15,* 346-352.

Miralles, D. G., Gentine, P., Seneviratne, S. I., & Teuling, A. J. (2019). Land-Atmospheric Feedbacks during Droughts and Heatwaves: State of the Science and Current Challenges. *Annals of the New York Academy of Sciences, 1436,* 19-35. https://doi.org/10.1111/nyas.13912

Myers, T. A., Scott, R. C., Zelinka, M. D., Klein, S. A., Norris, J. R., & Caldwell, P. M. (2021). Observational Constraints on Low Cloud Feedback Reduce Uncertainty of Climate Sensitivity. *Nature Climate Change, 11,* 501-507. https://doi.org/10.1038/s41558-021-01039-0

Nicholson, S. E. (2017). Climate and Climatic Variability of Rainfall over Eastern Africa. *Reviews of Geophysics, 55,* 590-635. https://doi.org/10.1002/2016rg000544

Nkunzimana, A. et al. (2021). Understanding the Complex Influences of Climatic and Non-Climatic Factors on Maize Yields in East Africa. *Theoretical and Applied Climatology, 145,* 1147-1167.

Ogwang, B. A., Ongoma, V., & Xing, L. (2021). The Influence of Indian Ocean Dipole on East African Rainfall. *Natural Hazards, 107,* 697-711.

Omondi, P. A., Awange, J. L., Forootan, E., Ogallo, L. A., Barakiza, R., Girmaw, G. B. et al. (2014). Changes in Temperature and Precipitation Extremes over the Greater Horn of

Africa Region from 1961 to 2010. *International Journal of Climatology, 34,* 1262-1277. https://doi.org/10.1002/joc.3763

Ongoma, V., Chen, H., & Gao, C. (2018). Projected Changes in Mean Rainfall and Temperature over East Africa Based on CMIP5 Models. *International Journal of Climatology, 38,* 1375-1392. https://doi.org/10.1002/joc.5252

Osima, S., Indasi, V. S., Zaroug, M., Endris, H. S., Gudoshava, M., Misiani, H. O. et al. (2018). Projected Climate over the Greater Horn of Africa under 1.5 °C and 2 °C Global Warming. *Environmental Research Letters, 13,* Article 065004. https://doi.org/10.1088/1748-9326/aaba1b

Perkins-Kirkpatrick, S. E., & Gibson, P. B. (2017). Changes in Regional Heatwave Characteristics as a Function of Increasing Global Temperature. *Scientific Reports, 7,* Article No. 12256. https://doi.org/10.1038/s41598-017-12520-2

Rasmijn, L. M., van der Schrier, G., Bintanja, R., Barkmeijer, J., Sterl, A., & Hazeleger, W. (2018). Future Equivalent of 2010 Russian Heatwave Intensified by Weakening Soil Moisture Constraints. *Nature Climate Change, 8,* 381-385. https://doi.org/10.1038/s41558-018-0114-0

Rowhani, P., Lobell, D. B., Linderman, M., & Ramankutty, N. (2011). Climate Variability and Crop Production in Tanzania. *Agricultural and Forest Meteorology, 151,* 449-460. https://doi.org/10.1016/j.agrformet.2010.12.002

Schreck, C. J., & Semazzi, F. H. M. (2004). Variability of the Recent Climate of Eastern Africa. *International Journal of Climatology, 24,* 681-701. https://doi.org/10.1002/joc.1019

Seneviratne, S. I., Corti, T., Davin, E. L., Hirschi, M., Jaeger, E. B., Lehner, I. et al. (2010). Investigating Soil Moisture-Climate Interactions in a Changing Climate: A Review. *Earth-Science Reviews, 99,* 125-161. https://doi.org/10.1016/j.earscirev.2010.02.004

Taylor, C. M., de Jeu, R. A. M., Guichard, F., Harris, P. P., & Dorigo, W. A. (2012). Afternoon Rain More Likely over Drier Soils. *Nature, 489,* 423-426. https://doi.org/10.1038/nature11377

Trenberth, K. E., Fasullo, J. T., & Kiehl, J. (2009). Earth's Global Energy Budget. *Bulletin of the American Meteorological Society, 90,* 311-324. https://doi.org/10.1175/2008bams2634.1

von Storch, H., & Zwiers, F. W. (1999). *Statistical Analysis in Climate Research* (484 p). Cambridge University Press. https://doi.org/10.1017/cbo9780511612336

Wilks, D. S. (2011). *Statistical Methods in the Atmospheric Sciences* (3rd ed.). Academic Press. https://doi.org/10.1016/b978-0-12-385022-5.00001-4

Xie, P., Chen, M., Yang, S., Yatagai, A., Hayasaka, T., Fukushima, Y. et al. (2007). A Gauge-Based Analysis of Daily Precipitation over East Asia. *Journal of Hydrometeorology, 8,* 607-626. https://doi.org/10.1175/jhm583.1